




Correlation of microstructure and magnetic properties in $\text{Sm}(\text{Co}_{\text{bal}}\text{Fe}_{0.1}\text{Cu}_{0.1}\text{Zr}_{0.033})_{6.93}$ magnets solution-treated at different temperatures

Cheng Xu, Hui Wang* , Tian-Li Zhang, Alexander Popov, Raghavan Gopalan, Cheng-Bao Jiang

Received: 18 July 2018 / Revised: 13 October 2018 / Accepted: 30 October 2018 / Published online: 6 December 2018
© The Nonferrous Metals Society of China and Springer-Verlag GmbH Germany, part of Springer Nature 2018

Abstract The correlation of microstructure and magnetic properties in $\text{Sm}(\text{Co}_{\text{bal}}\text{Fe}_{0.1}\text{Cu}_{0.1}\text{Zr}_{0.033})_{6.93}$ magnets solution-treated at different temperatures was systematically investigated. It is found that the magnets solution-treated at 1219 °C possess a single 1:7H phase, exhibiting the homogeneous cellular structure during further aging treatment, leading to the optimum magnetic properties. However, for the magnets solution-treated at 1211 and 1223 °C, 2:17R or 1:5H secondary phase will also form besides 1:7H main phase, which cannot transform into cellular structure, thus deteriorating the magnetic properties greatly. The irreversible magnetization investigations with recoil loops also propose a non-uniform pinning in the magnets induced by the secondary precipitates. At proper solution temperature, Zr is supposed to occupy the Fe–Fe dumbbell sites in the form of Zr-vacancy pairs, leading to the minimum c/a ratio and thus stabilizing the 1:7H phase. Finally, $\text{Sm}(\text{Co}_{\text{bal}}\text{Fe}_{0.1}\text{Cu}_{0.1}\text{Zr}_{0.033})_{6.93}$ magnets with the maximum energy product and intrinsic coercivity at 550 °C up to 60.73 kJ·m⁻³ and 553.88 kA·m⁻¹ were prepared by powder metallurgy method.

Keywords $\text{Sm}_2\text{Co}_{17}$; Solution treatment; Phase constitution; Demagnetization curve squareness

1 Introduction

High-temperature permanent magnets capable of operating at 550 °C have attracted great interest due to the application as critical components for aviation devices and micro-electro-mechanical systems, i.e., microwave tubes, magnetic bearings, sensors and actuators [1–8]. Among which, precipitation-hardened $\text{Sm}_2\text{Co}_{17}$ -based permanent magnets are well known to have outstanding magnetocrystalline anisotropy, high Curie temperature and low temperature coefficient of coercivity and remanence, and are considered to be the most potential material as high-temperature permanent magnets [9–11]. Therefore, intensive studies have been focused on the improvement in the magnetic properties at 550 °C in $\text{Sm}_2\text{Co}_{17}$ -based magnets [12–15].

The preparation of $\text{Sm}_2\text{Co}_{17}$ -type magnets needs to adopt a long-time heat treatment including sintering, solution treatment, isothermal aging and slow cooling treatment. The pyramid-shaped cellular structure is developed after the above complex heat treatment, accompanied with the emergence of platelet Zr-rich phase parallel to 2:17R basal plane [16]. The nanoscale cellular structure consists of 2:17R phase as the cell and 1:5H phase as the cell boundary [17]. The microchemistry evolution inside the unique cellular structure during isothermal treatment, i.e., the formation of the Fe-rich cell and the Cu-rich cell boundary, is responsible for the generation of the good combination of the magnetic properties (saturation magnetization, intrinsic coercivity, etc.) [18–21].

Over the last decade, the relationship between the aging regime and magnetic properties has got tremendous

C. Xu, H. Wang*, T.-L. Zhang, C.-B. Jiang
School of Materials Science and Engineering, Beihang University, Beijing 100191, China
e-mail: huiwang@buaa.edu.cn

A. Popov
M. N. Miheev Institute of Metal Physics, Ural Branch of Russian Academy of Sciences, Ekaterinburg, Russia 620990

R. Gopalan
International Advanced Research Centre for Powder Metallurgy and New Materials (ARCI), IITM Research Park, Chennai 600113, India

attention in order to understand the coercivity mechanism during isothermal aging [22, 23]. Furthermore, the magnetic properties, especially the squareness and knee point in the second-quadrant demagnetization curve, are sensitively dependent on the solution treatment temperature, and hence it is extremely important to investigate the correlation of microstructure and magnetic properties in $\text{Sm}_2\text{Co}_{17}$ -based magnets during solution treatment. However, until now the recognition of the solution structure remains ambiguous. Morit et al. [24] proposed that the structure of the solution-treated sample depends on the content of Cu, Fe, Zr, as well as the solution treatment temperature. Livingston and Martin [25] suggested a disordered hexagonal SmCo_5 phase for the solution structure, among which 29% of the Sm sites are randomly replaced by transition-metal pairs. It was proposed that the high-temperature phase should be hexagonal TbCu_7 -type structure (1:7H phase) with partial ordered 2:17R-type structure as the stoichiometric ratio within 1/5–2/17, depending on the cooling rate of quenching during investigation [26–28]. However, Ray et al. [10, 29–31] assumed that the solution state is partially disordered 2:17R phase, in which the addition of Zr can stabilize the 2:17R structure for the magnets with high Fe concentrations by displacing the Fe–Fe dumbbell pairs with Zr–vacancy pairs. Gopalan et al. [32, 33] have reported that the solution-treated sample structure should be 1:7H for the Sm-rich composition, while be 2:17H structure for the Sm-poor composition, which cannot be translated into cellular structure after aging treatment. Furthermore, it is suggested the magnets comprising TbCu_7 structure quenched from the solution temperature can possess high coercivity after aging treatment [24]. Therefore, the solution treatment is necessary to form a homogeneous microstructure and uniform fine magnetic domain structure in order to obtain excellent performance [32–34]. Recently, it is found that special solution treatments for homogenization during preparation of $\text{Sm}_2\text{Co}_{17}$ -based magnets are beneficial for the improvement in magnetic product [35, 36].

According to the above discussion, the solution structure is supposed to be sensitive to the solution treatment temperature as well as Sm composition in $\text{Sm}_2\text{Co}_{17}$ magnet. However, the structure remains ambiguous, and also the relationship between the magnetic properties and structure as well as solution treatment needs to be clarified. In this paper, the microstructures of solution-treated $\text{Sm}_2\text{Co}_{17}$ -type high-temperature magnets heat-treated at different solution temperatures were investigated systematically. The influence of the solution temperature on the microstructure as well as the magnetic properties, especially the squareness or knee point in the second-quadrant demagnetization curves of $\text{Sm}_2\text{Co}_{17}$ magnets, was

analyzed. The correlation between solution-treated structure and the magnetic properties was proposed.

2 Experimental

The alloy with nominal composition of $\text{Sm}(\text{Co}_{\text{bal}}\text{Fe}_{0.1}\text{Cu}_{0.1}\text{Zr}_{0.033})_{6.93}$ was prepared by arc melting 99.5% pure elements under an argon atmosphere. The ingots were crushed and ground to less than 200 μm . Subsequently, the crushed ingots were ball-milled into powders with an average particle size of 3–5 μm . The powders were then aligned in a magnetic field and compacted into green bodies by cold isostatic pressing. The compacted samples were initially sintered at 1210–1230 $^{\circ}\text{C}$ for 1 h, solution-treated at 1210–1225 $^{\circ}\text{C}$ for 4 h and then water-quenched to room temperature. Subsequently, the solution-treated samples were isothermally treated at 800–820 $^{\circ}\text{C}$ for 24 h, slowly cooled to 400 $^{\circ}\text{C}$, held at 400 $^{\circ}\text{C}$ for 10 h and then water-quenched to room temperature. The demagnetization curves were measured by NIM-500C B–H tracer after the samples were magnetized at a field of 10 T. The phase constitution was analyzed by a Rigaku D/max2500PC X-ray diffractometer (XRD) with $\text{Cu K}\alpha$ radiation. The microstructure and composition analysis were conducted by JXA-8100 electron probe microanalyzer (EPMA) and JEM-2100F transmission electron microscope (TEM) equipped with energy-dispersive spectrometer (EDS). The oxygen content was measured using O-3000 Infrared Oxygen Analyzer. The hysteresis loops and recoil loops in the initial magnetization and demagnetization state were recorded by a physical property measurement system (PPMS).

3 Results and discussion

Figure 1 shows demagnetization curves of isothermally aged and slowly cooled magnets after solution-treated at 1211, 1215, 1219 and 1223 $^{\circ}\text{C}$, respectively. As can be seen from Fig. 1a, there exists a “knee point” in the demagnetization curves of 1211 and 1215 $^{\circ}\text{C}$ solution-treated samples, which is considered to result from two uncoupled magnetic phases [37]. The existence of the knee point inevitably deteriorates the squareness of the demagnetization curve and leads to the degradation of the magnetic properties. When the magnets were solution-treated at 1219 $^{\circ}\text{C}$, both the squareness and the magnetic energy product are greatly improved. Figure 1b, c summarizes the dependence of magnetic properties (remanence, B_r ; intrinsic coercivity, ${}_{i}H_c$; squareness factor, $H_k/{}_{i}H_c$; the maximum energy product, $(BH)_{\text{max}}$) on solution treatment temperature. The magnetic properties, such as the

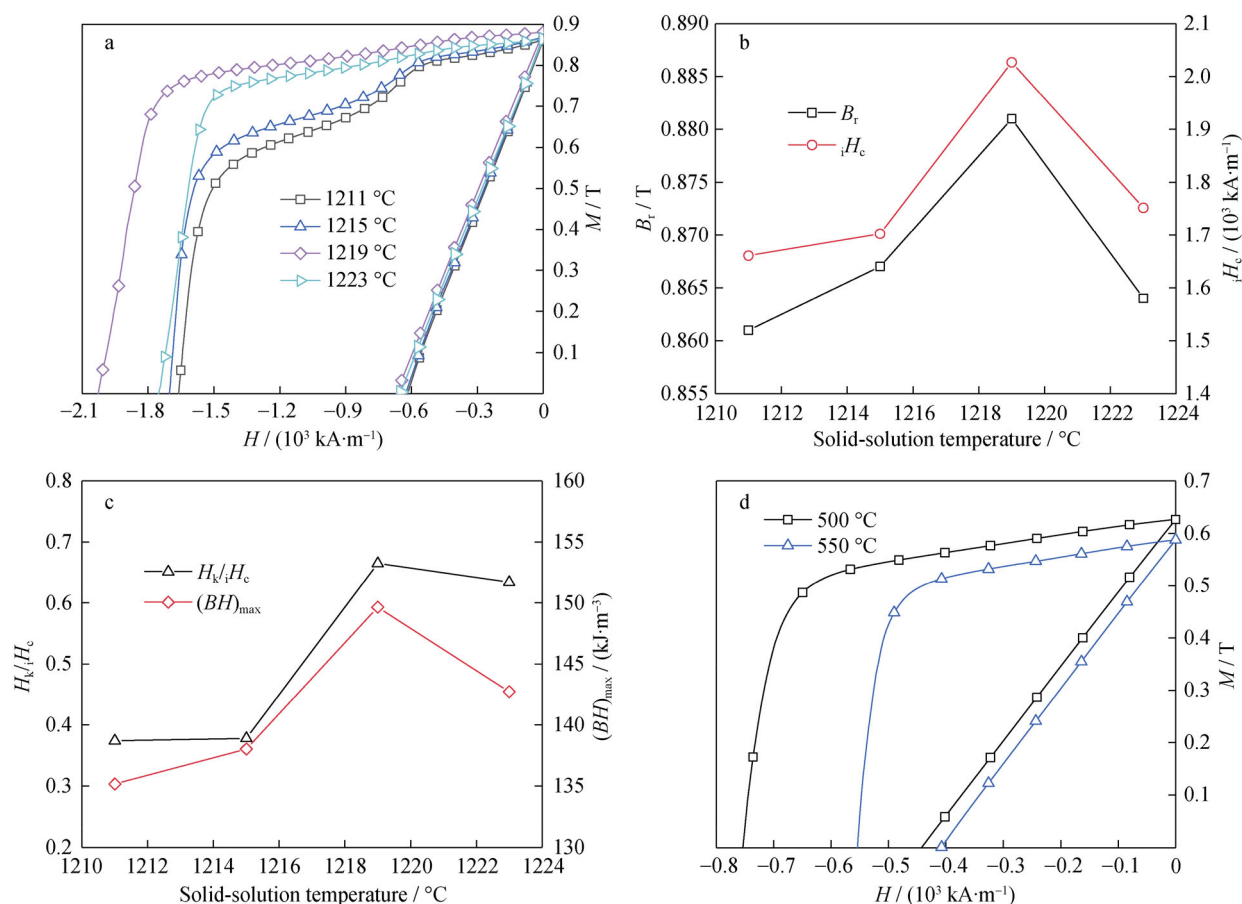


Fig. 1 a Demagnetization curves of as-aged magnets solution-treated at different temperatures; variation of **b** B_r , iH_c and **c** H_k/iH_c , $(BH)_{\text{max}}$ with solution temperatures; **d** 500 and 550 °C demagnetization curve of magnet optimally solution-treated at 1219 °C

maximum energy product, intrinsic coercivity and squareness, are improved to $149.65 \text{ kJ}\cdot\text{m}^{-3}$, $2026.90 \text{ kA}\cdot\text{m}^{-1}$ and 0.665, respectively, for magnets solution-treated at 1219 °C, with a slightly higher B_r of 0.881 T than the magnets solution-treated at other temperatures. Figure 1d shows the 500 and 550 °C magnetic properties of the magnet solution-treated at 1219 °C. The energy product at 550 °C reaches $60.73 \text{ kJ}\cdot\text{m}^{-3}$, and the intrinsic coercivity reaches $553.88 \text{ kA}\cdot\text{m}^{-1}$, indicating that the magnet with composition $\text{Sm}(\text{Co}_{\text{bal}}\text{Fe}_{0.1}\text{Cu}_{0.1}\text{Zr}_{0.033})_{6.93}$ has a potential capability using at 550 °C.

XRD patterns of the magnets treated at different solution treatment temperatures are shown in Fig. 2a. It can be seen that the phase constitutions vary with the solution temperature. The solid solution is found to be composed of disordered 1:7H phase and 2:17H phase for magnets solution-treated at 1211 and 1215 °C. For the magnets solution-treated at 1219 °C, the (203) peak of the 2:17H is absent, indicating the formation of 1:7H single phase. When the solution temperature increases to 1223 °C, the (203) peak of 2:17H appears again along with 1:7H phase. Besides, the diffraction peaks of 1:7H phase in the samples

solution-treated at 1219 °C shift to right side in XRD pattern. Figure 2b, c shows the lattice constants calculated from XRD patterns with different solution temperatures. The lattice constant a of the 1:7H phase increases with solution temperature initially increasing, reaching the maximum at 1219 °C, and then decreases as the solution temperature increases to 1223 °C. On the other hand, the lattice constant c has an opposite variation tendency, illustrating that there exists a shrinkage below 1219 °C and expansion at 1223 °C. As a consequence, the c/a value exhibits the same changing tendency as the lattice constant c (Fig. 2c).

Figure 3a–d shows the back-scattered electron (BSE) images of the magnets solution-treated at 1211–1223 °C, respectively. The phase with the brightest contrast in all samples is identified as Sm_2O_3 , resulting from the inevitable oxidation during ball milling and sintering. The large gray areas correspond to the main phase 1:7H. The phase showing dark contrast in the magnets solution-treated at 1211 and 1215 °C is identified to be $\text{Zr}_6(\text{Fe},\text{Co})_{23}$ phase according to the composition analysis. While for the magnet solution-treated at 1219 °C, rarely $\text{Zr}_6(\text{Fe},\text{Co})_{23}$

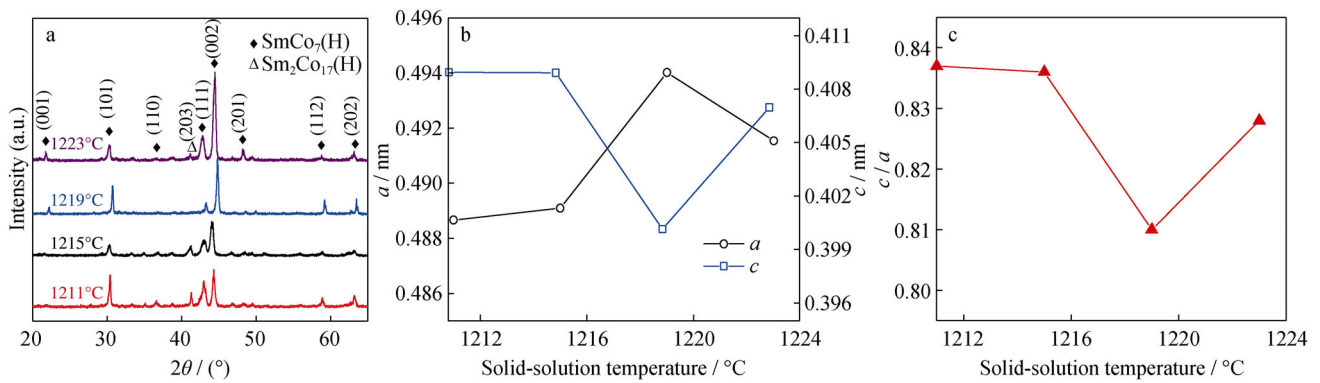


Fig. 2 a XRD patterns of magnets solution-treated at different temperatures; lattice parameters variation of **b** a , c and c/a with solution temperature calculated from XRD results

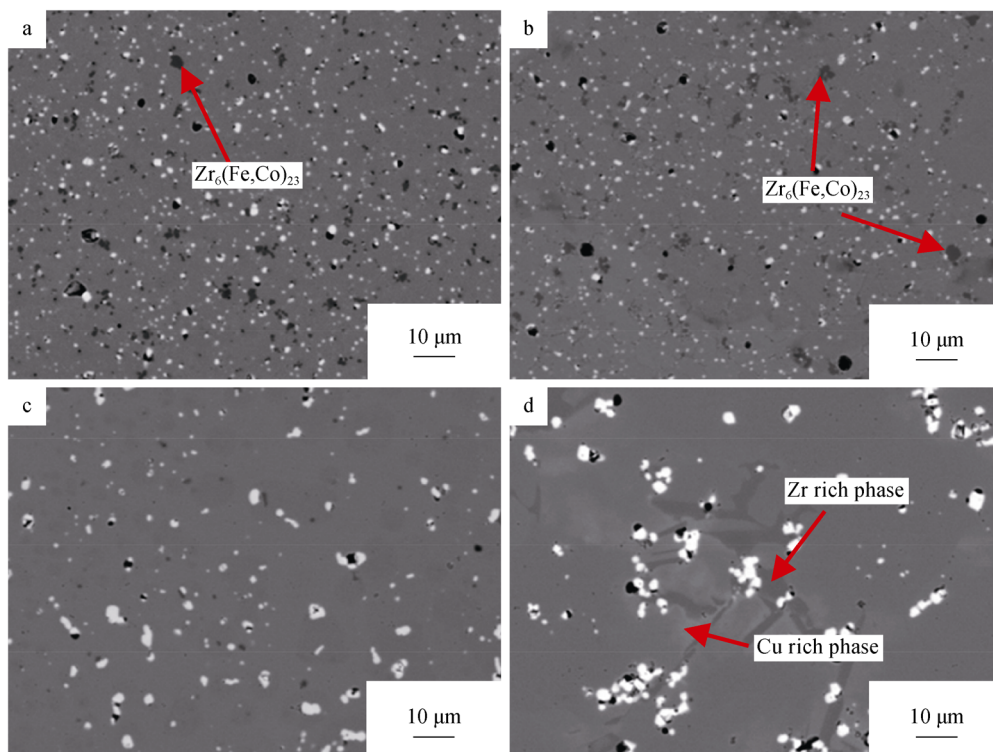


Fig. 3 BSE images of magnets treated at different solution temperatures: **a** 1211 °C, **b** 1215 °C, **c** 1219 °C, **d** 1223 °C and quenched

can be observed. The $\text{Zr}_6(\text{Fe,Co})_{23}$ phase has also been reported in $\text{Sm}_2\text{Co}_{17}$ -type magnets with higher Fe contents, which is supposed to result from the excess addition of Zr in the quinary alloy or the insufficient solution treatment process [9, 33, 36]. Contrary to the expectation, no apparent contrast exists for the $\text{Sm}_2\text{Co}_{17}(\text{H})$ phase for the samples solution-treated at 1211 and 1215 °C, which can be attributed to the minor composition difference between 2:17H and 1:7H. The existence of 2:17H will be confirmed by TEM in the further discussion.

It can be noticed that no extra peaks exist for Sm_2O_3 and $\text{Zr}_6(\text{Fe,Co})_{23}$ in XRD patterns (Fig. 2a), which seems to

contradict the microstructure observations shown in Fig. 3a, b. According to the oxygen analysis results, the oxygen content of as-aged magnet solution-treated at 1211 °C is 0.3 wt%. The content of Sm_2O_3 can be deduced from the oxygen content as 2.57 vol%. The contents of Sm_2O_3 and $\text{Zr}_6(\text{Fe,Co})_{23}$ in as-aged magnets solution-treated at 1211 °C are also calculated according to BSE image (Fig. 3a), which are 2.6 vol% and 2.8 vol%, respectively. The calculated content of Sm_2O_3 coincides with the measured value. Due to minor contents of Sm_2O_3 and $\text{Zr}_6(\text{Fe,Co})_{23}$, they can hardly be distinguished from XRD patterns.

As Fig. 3c shows, the as-solutioned magnet at 1219 °C has a pure and single main phase, characterized as 1:7H by XRD patterns. There is a marked change for the solution-treated magnet at 1223 °C as shown in Fig. 3d. A secondary phase in darker contrast with a strip shape precipitates from the gray main phase. Meanwhile, there exists an obscure local irregularity surrounding the dark gray phase, which has a light gray contrast. According to the composition analysis, the dark gray phase and light gray phase are Sm-poor/Zr-rich phase and Sm/Cu-rich phase, respectively. The existence of the secondary phases may be the cause of the slight deterioration of the squareness in the second-quadrant demagnetization curve compared with the as-aged magnets solution-treated at 1219 °C.

Figures 4 and 5 show the elemental mapping of the magnets solution-treated at 1211 and 1223 °C analyzed by EPMA. Obviously, the Zr-rich secondary phases precipitate in these two situations. The precipitations of Zr-rich secondary phases imply that the solution of Zr in the magnets is sensitive to the solution temperature. As the solution temperature is below 1219 °C, the Zr-rich $Zr_6(Fe,Co)_{23}$ phase precipitates out, while the solution temperature increases above 1219 °C, the main phase decomposes into Zr-rich and Sm/Cu-rich phases, as described in Fig. 3d. According to the elemental analysis

results, the Sm/Cu-rich phase has the composition close to that of 1:5 and Zr-rich phase is close to 2:17 stoichiometric proportion. The precise characterization of the precipitates will be discussed using TEM analysis.

As shown in Fig. 2b, c, the lattice constants vary with different solution temperatures, which can be directly related to the atomic type occupied in the crystal cells. According to the model proposed by Ray, Zr has the effect to stabilize the high-temperature 2:17R disordered phase by replacing Fe–Fe dumbbell pairs with Zr-vacancy pairs parallel to the *c*-axis [29, 38], which will lead to an expansion in *a*-axis and shrinkage in *c*-axis simultaneously. Analogously, it is supposed that for the magnets solution-treated at 1219 °C, the sufficient solution treatment boosts enough Zr-vacancy pairs occupying the Fe–Fe dumbbell sites in $SmCo_7(H)$ phase, leading to the minimum *c/a* and inhibiting the precipitation of $Zr_6(Fe,Co)_{23}$ phase, which is consistent with the composition analysis and the lattice parameters variation.

Figure 6a, b shows a TEM morphology of the magnets solution-treated at 1211 °C and its corresponding selected area electron diffraction (SAED) patterns. It can be seen from Fig. 6a that a small grain with a width of $\sim 1 \mu m$ embeds in the surroundings of some bigger grains. The corresponding SAED patterns viewing from [010] zone

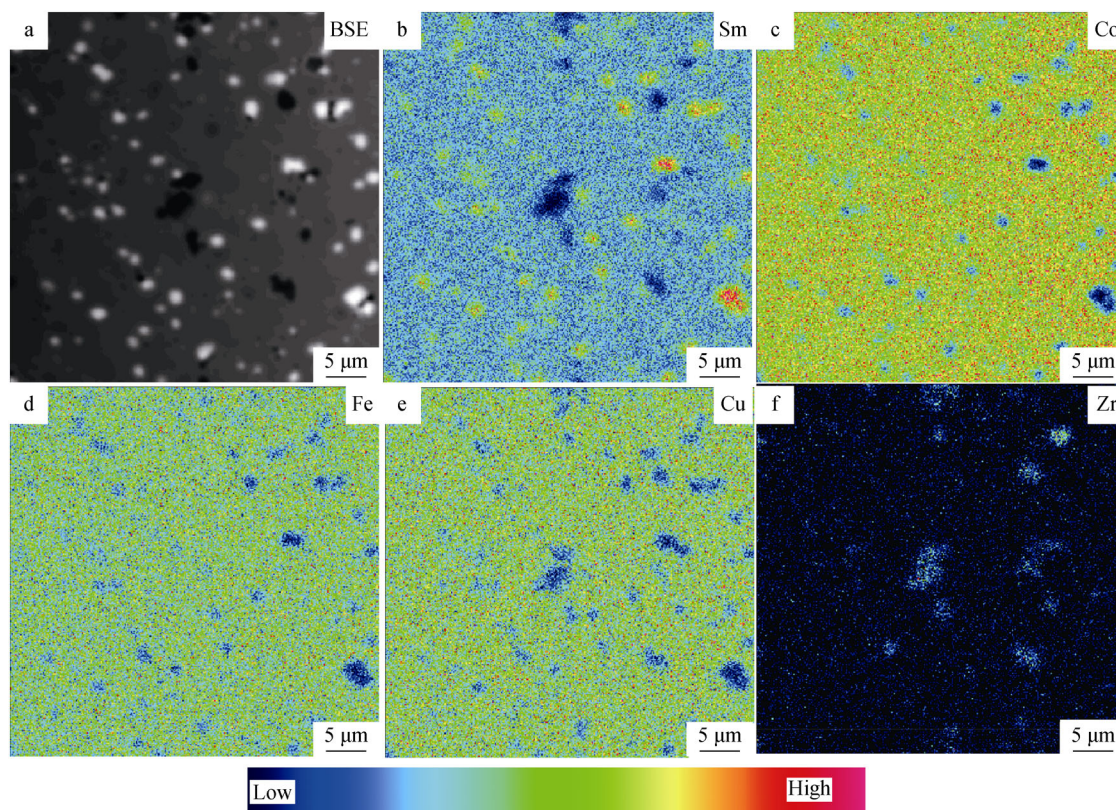


Fig. 4 a BSE image and EPMA mapping images of b Sm, c Co, d Fe, e Cu, f Zr obtained from samples solution-treated at 1211 °C

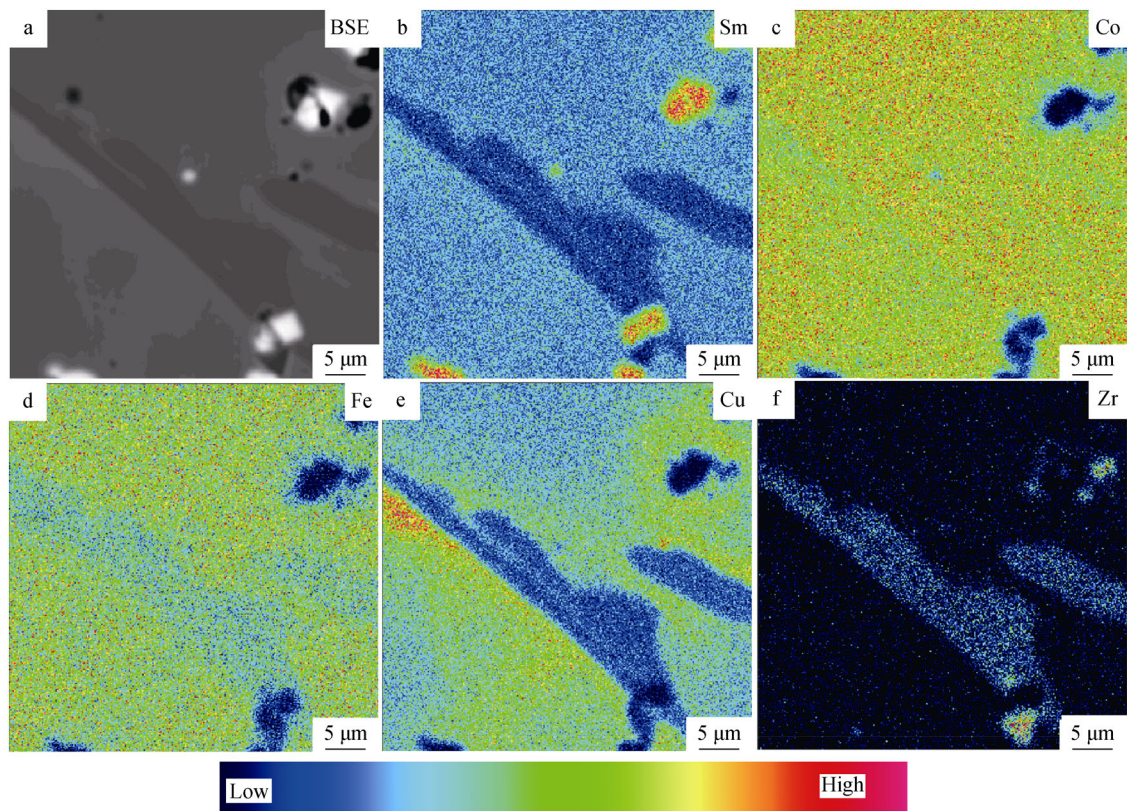


Fig. 5 a BSE image and EPMA mapping images of b Sm, c Co, d Fe, e Cu, f Zr obtained from samples solution-treated at 1223 °C

axis show the occurrence of $\{101\}$ and $\{201\}$ superlattice reflections (Fig. 6b), which clearly demonstrates the existence of 2:17H phase. Figure 6c–e displays the microstructure of the secondary phase in the magnets solution-treated at 1223 °C and its corresponding SAED patterns. The strip-shaped phase corresponds to the Zr-rich phase with surrounding grains containing a large amount of Cu, confirmed by EDS results shown in Fig. 6f. SAED patterns of the Zr-rich phase and Cu-rich phase in Fig. 6d, e are indexed to be 1:5H and 2:17H phases, with the zone axis indexed as $[210]$ and $[1\bar{2}0]$, respectively. These results are well consistent with EPMA results. According to above analysis, with sufficient Zr substitution for Fe–Fe dumbbells, the disordered 1:7H remains stable as the solution-treated structure. However, for the magnets solution-treated at temperature below or above 1219 °C, the precipitation of Zr-rich secondary phase results in partial of the solution structure transforming from 1:7H into 2:17H or 1:5H phase.

Figure 7 shows the microstructures of the as-aged magnets with the nominal c -axis of the $\text{Sm}_2\text{Co}_{17}(\text{R})$ phase parallel or perpendicular to the electron beam incident direction. It is well known that the cellular/lamellar structures with proper microchemistry develop when the solution-treated magnets are subjected to the aging treatment.

The as-aged magnets consist of ~ 70 nm cellular structure with platelet phase running across the cells. However, the precipitations lead to the formation of uneven structures in local regions. As for the isothermally aged magnets which are initially solution-treated at 1211 °C, the 2:17H secondary phase transforms into 2:17R without element diffusion to form 1:5H cell boundary during the aging treatment. As Fig. 7b shows, there exists a grain containing large scales of 2:17R with twin structure in the magnets. The inhomogeneity of the cellular structure is also discovered in the magnets solution-treated at 1223 °C as presented in Fig. 7e. While for the magnets solution-treated at 1219 °C, the single 1:7H phase will transform to cellular 2:17R phase and 1:5 cell boundary phase after aging treatment (Fig. 7c, d).

The magnetization behaviors of the as-aged magnets treated with different solution temperatures are studied thoroughly. The recoil curves have been employed to measure the irreversible magnetization, and the detail of this method is described in Refs. [39–41]. As shown in Fig. 8a, the irreversible magnetization (M_{irr}) of the as-aged magnets solution-treated at 1211 °C increases more rapidly at the field $H/H_c < 1$ than that of magnets solution-treated at 1219 °C. This suggests that the demagnetization process is easier for the magnets solution-treated at 1211 °C due to

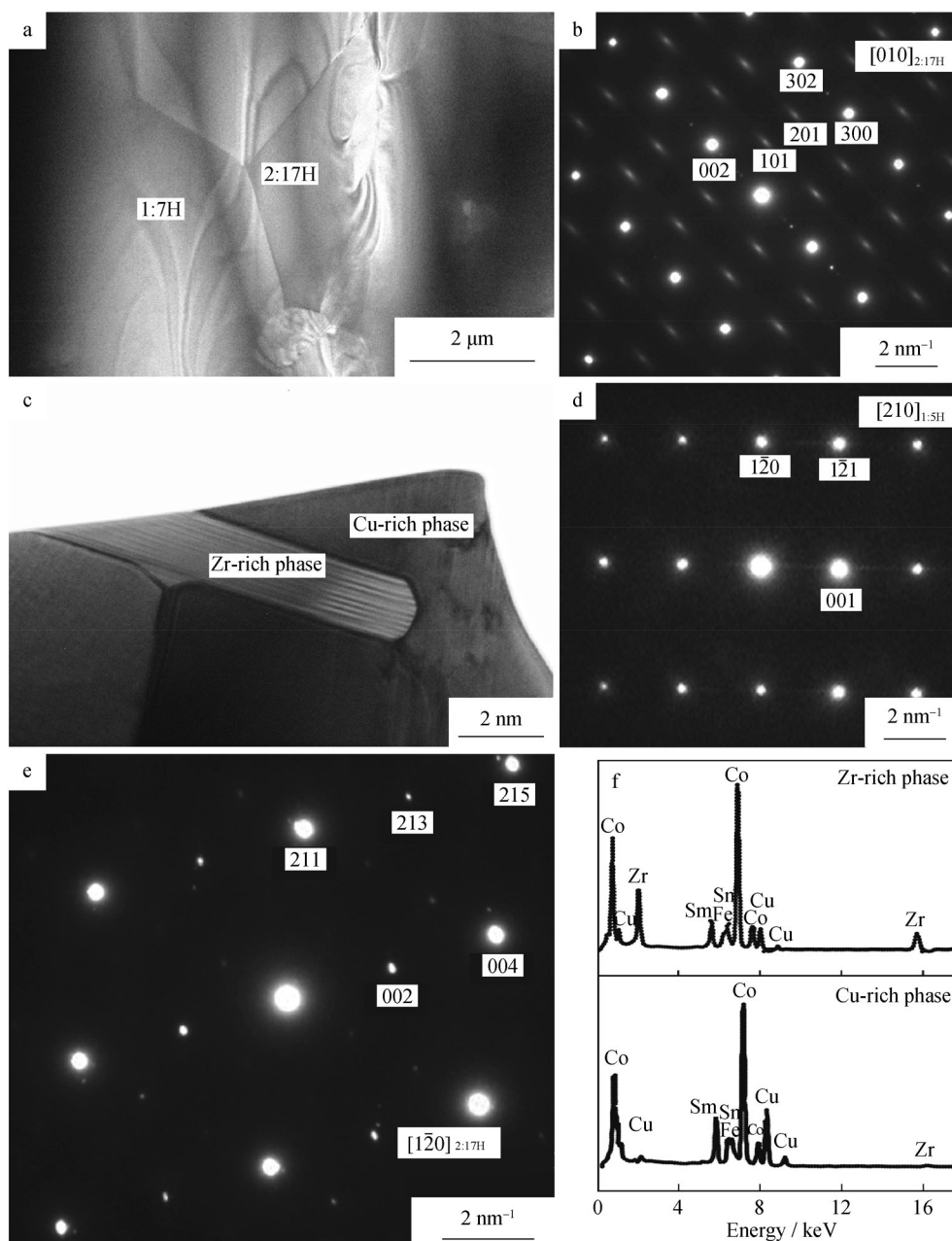


Fig. 6 **a** TEM image of magnets solution-treated at 1211 °C and **b** SAED patterns showing 2:17H structure illustrated in **a**, with appearance of {101} and {201} superlattice reflections; **c** TEM image of magnets solution-treated at 1223 °C and quenched; SAED patterns indexed as **d** 1:5H and **e** 2:17H phase, corresponding to Zr-rich and Cu-rich phase shown in **c**; **f** EDS spectra showing Zr-rich and Cu-rich particles in **c**

the existence of softer secondary phase, such as 2:17R twinning structure in as-aged magnets. As shown in Fig. 8b, the curve of irreversible magnetization susceptibility (χ_{irr}) of as-aged magnets solution-treated at 1211 °C has two peaks during the demagnetization process, which can be considered as two magnetic-phase behaviors. Furthermore, the shape of the peaks corresponding to the magnets treated at 1211 °C is lower and wider, implying that the irreversible field is broad and non-uniform, which causes the squareness deterioration of the demagnetization

curves in the second quadrant. The relatively larger irreversible magnetization susceptibility for samples solution-treated at 1219 °C reflects the much stronger coupling between 2:17R cell phase and 1:5H cell boundary phase. As illustrated in Fig. 7b, e, the twinning structure and non-uniform cellular structures in as-aged magnets solution-treated at 1211 °C or 1223 °C will deteriorate the effective pinning strength. For the magnets solution-treated at 1219 °C, the uniform cellular structure derived from the

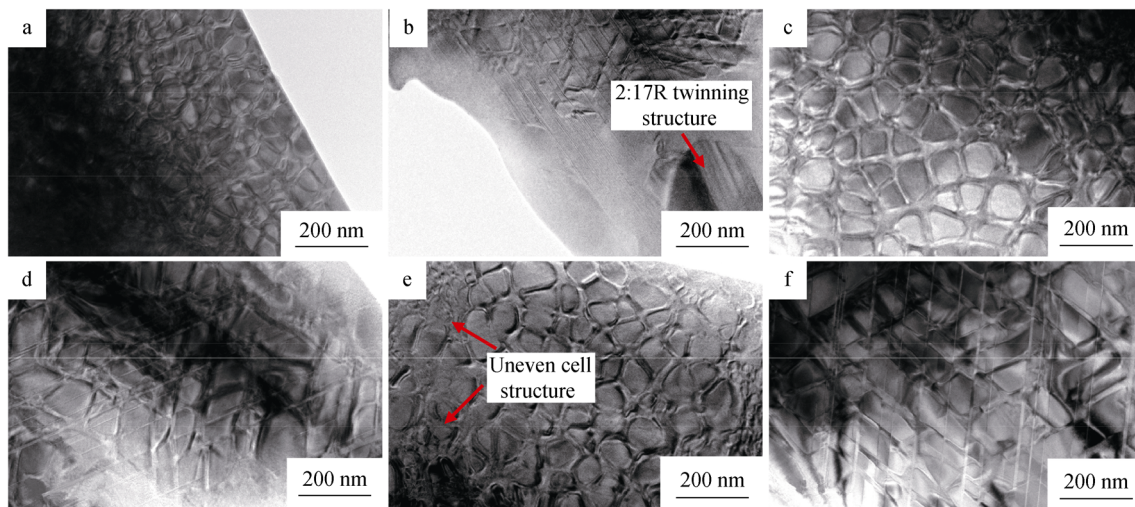


Fig. 7 TEM images of as-aged magnets solution-treated at **a, b** 1211 °C, **c, d** 1219 °C, **e, f** 1223 °C with nominal *c*-axis of 2:17R main phase perpendicular (**a, c, e**) and parallel (**b, d, f**) to electron incidence

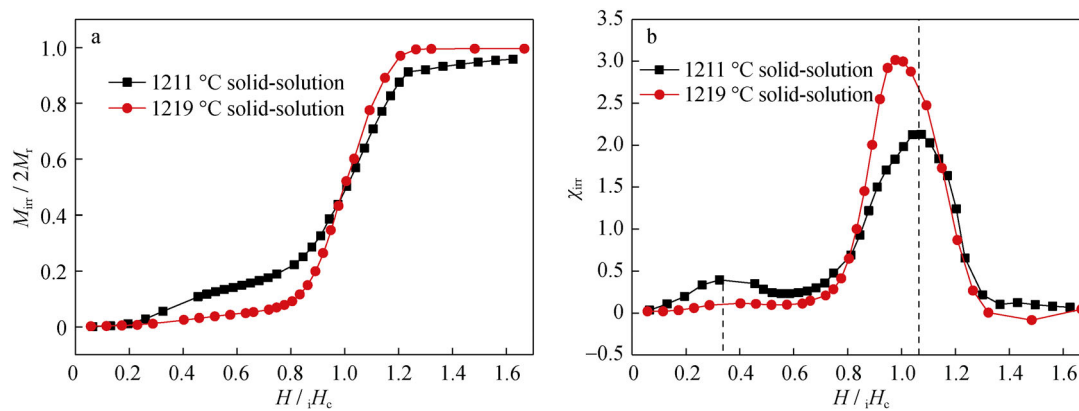


Fig. 8 **a** Irreversible magnetization and **b** irreversible magnetization susceptibility of as-aged magnets solution-treated at 1211 and 1219 °C

single-phase 1:7H is the key factor for the magnets acquiring high coercivity and squareness.

4 Conclusion

In conclusion, $\text{Sm}(\text{Co}_{\text{bal}}\text{Fe}_{0.1}\text{Cu}_{0.1}\text{Zr}_{0.033})_{6.93}$ high-temperature permanent magnets were prepared by optimal process, with energy product and intrinsic coercivity at 550 °C up to $60.73 \text{ kJ}\cdot\text{m}^{-1}$ and $553.88 \text{ kA}\cdot\text{m}^{-1}$, respectively. The magnetic properties are sensitive to the solution temperatures, which influence the solution structures and phase constitutions in magnets. The single-phase 1:7H can be obtained at the optimum solution temperature of 1219 °C, which promotes the solution of Zr in the 1:7H, stabilizing the disordered 1:7H and avoiding the precipitation of secondary phases. While for the magnets solution-treated at 1211 °C or 1223 °C, the secondary phases such as 2:17H or 1:5H transform into 2:17R phase with twinning structure

during aging treatment. These will result in non-uniform and broad pinning field, which is responsible for the deterioration of squareness in the second-quadrant demagnetization curves and thus the magnetic properties.

Acknowledgements This study was financially supported by the National Natural Science Foundation of China (No. 51471016), the Natural Science Foundation of Beijing (No. 2151002), and the BRICS STI Framework Program (Nos. 51761145026 and 17-52-80072). The author Raghavan Gopalan from India thanks Department of Science and Technology, Govt of India, for supporting the work under DST-BRICS proposal reg. No 258.

References

- [1] Pathak AK, Khan M, Gschneidner KA, McCallum RW, Zhou L, Sun K, Dennis KW, Zhou C, Pinkerton FE, Kramer MJ. Cerium: an unlikely replacement of dysprosium in high performance Nd-Fe-B permanent magnets. *Adv Mater.* 2015;27(16):2663.
- [2] Gutfleisch O, Müller KH, Khlopkov K, Wolf M, Yan A, Schäfer R, Gemming T, Schultz L. Evolution of magnetic domain

- structures and coercivity in high-performance SmCo 2:17-type permanent magnets. *Acta Mater.* 2006;54(4):997.
- [3] Gutfleisch O, Willard MA, Brück E, Chen CH, Sankar S, Liu JP. Magnetic materials and devices for the 21st century: stronger, lighter, and more energy efficient. *Adv Mater.* 2011;23(7):821.
 - [4] Kumar S, Kumar R, Chakarvarti S. Morphological and magnetic characterization of electrodeposited cobalt nanowires. *J Mater Sci.* 2004;39(8):2951.
 - [5] Saini D, Chauhan R, Kumar S. Effects of annealing on structural and magnetic properties of template synthesized cobalt nanowires useful as data storage and nano devices. *J Mater Sci Mater Electron.* 2014;25(1):124.
 - [6] An S, Zheng L, Zhang T, Jiang C. Bulk anisotropic nanocrystalline SmCo_{6.6}Ti_{0.4} permanent magnets. *Scr Mater.* 2013;68(6):432.
 - [7] Ma Z, Zhang T, Jiang C. A facile synthesis of high performance SmCo₅ nanoparticles. *Chem Eng.* 2015;264:610.
 - [8] Ma Z, Zhang T, Jiang C. Exchange-coupled SmCo₅/Co nanocomposites synthesized by a novel strategy. *RSC Adv.* 2015;5(108):89128.
 - [9] Hadjipanayis GC. Magnetic hardening in Zr-substituted 2:17 rare-earth permanent magnets. *J Appl Phys.* 1984;55(6):2091.
 - [10] Ray A. The development of high energy product permanent magnets from 2:17 RE-TM alloys. *IEEE Trans Magn.* 1984;20(5):1614.
 - [11] Zhang XF, Zhang WK, Li YF, Liu YL, Li ZB, Ma Q, Shi MF, Liu F. Magnetic properties of melt-spun MM-Fe-B ribbons with different wheel speeds and mischmetal contents. *Rare Met.* 2017;36(12):992.
 - [12] Yu N, Zhu M, Fang Y, Song L, Sun W, Song K, Wang Q, Li W. The microstructure and magnetic characteristics of Sm(Co_{bal}Fe_{0.1}Cu_{0.09}Zr_{0.03})_{7.24} high temperature permanent magnets. *Scr Mater.* 2017;132:44.
 - [13] Zhang T, Liu H, Liu J, Jiang C. 2:17-type SmCo quasi-single-crystal high temperature magnets. *Appl Phys Lett.* 2015;106(16):162403.
 - [14] Zhang T, Liu H, Ma Z, Jiang C. Single crystal growth and magnetic properties of 2:17-type SmCo magnets. *J Alloys Compd.* 2015;637:637.
 - [15] Wang Q, Zheng L, An S, Zhang T, Jiang C. Thermal stability of surface modified Sm₂Co₁₇-type high temperature magnets. *J Magn Magn Mater.* 2013;331:245.
 - [16] Mishra RK, Thomas G, Yoneyama T, Fukuno A, Ojima T. Microstructure and properties of step aged rare earth alloy magnets. *J Appl Phys.* 1981;52(3):2517.
 - [17] Rabenberg L, Mishra R, Thomas G. Microstructures of precipitation-hardened SmCo permanent magnets. *J Appl Phys.* 1982;53(3):2389.
 - [18] Jiang C, Hua H, Wang J. Thermomagnetic coupling martensitic transformation and associated physical effects. *Chin J Rare Met.* 2017;41(5):505.
 - [19] Romero S, de Campos M, de Castro J, Moreira A, Landgraf F. Microstructural changes during the slow-cooling annealing of nanocrystalline SmCo 2:17 type magnets. *J Alloys Compd.* 2013;551:312.
 - [20] Gopalan R, Ohkubo T, Hono K. Identification of the cell boundary phase in the isothermally aged commercial Sm(Co_{0.725}Fe_{0.1}Cu_{0.12}Zr_{0.04})_{7.4} sintered magnet. *Scr Mater.* 2006;54(7):1345.
 - [21] Gopalan R, Hono K, Yan A, Gutfleisch O. Direct evidence for Cu concentration variation and its correlation to coercivity in Sm(Co_{0.74}Fe_{0.1}Cu_{0.12}Zr_{0.04})_{7.4} ribbons. *Scr Mater.* 2009;60(9):764.
 - [22] Xiong X, Ohkubo T, Koyama T, Ohashi K, Tawara Y, Hono K. The microstructure of sintered Sm(Co_{0.72}Fe_{0.20}Cu_{0.05}Zr_{0.025})_{7.5} permanent magnet studied by atom probe. *Acta Mater.* 2004;52(3):737.
 - [23] Goll D, Kronmüller H, Stadelmaier H. Micromagnetism and the microstructure of high-temperature permanent magnets. *J Appl Phys.* 2004;96(11):6534.
 - [24] Mori Y, Umeda T, Kimura Y. Phase transformation at high temperature and coercivity of Sm (Co, Cu, Fe, Zr)₇₋₉ magnet alloys. *IEEE Trans Magn.* 1987;23(5):2702.
 - [25] Livingston J, Martin D. Microstructure of aged Sm(Co, Cu, Fe)₇ magnets. *J Appl Phys.* 1977;48(3):1350.
 - [26] Maury C, Rabenberg L, Allibert C. Genesis of the cell microstructure in the Sm (Co, Fe, Cu, Zr) permanent magnets with 2:17 type. *Phys Status Solidi A.* 1993;140(1):57.
 - [27] Fidler J, Bernardi J, Skalicky P. Analytical electron microscope study of high-and low-coercivity SmCo 2:17 magnets. *MRS Online Proc Libr.* 1987;96:181.
 - [28] Fidler J, Bernardi J, Ohashi K, Tawara Y. Analytical electron microscopy of Sm (Co, Fe, Cu, Zr)₉. *IEEE Trans Magn.* 1990;26(5):1385.
 - [29] Ray A. Metallurgical behavior of Sm (Co, Fe, Cu, Zr)_z alloys. *J Appl Phys.* 1984;55(6):2094.
 - [30] Ray AE, Soffa WA, Blachere JR, Zhang B. Cellular microstructure development in Sm(Co,Fe,Cu,Zr)_{8.35} alloys. *IEEE Trans Magn.* 1987;23(5):2711.
 - [31] Ray A. A revised model for the metallurgical behavior of 2:17-type permanent magnet alloys. *J Appl Phys.* 1990;67(9):4972.
 - [32] Gopalan R, Sastry T, Singh A, Chandrasekaran V. X-ray diffraction and microstructural studies in 2:17 type Sm-Co magnetic alloys containing Fe, Cu, and Zr. *J Mater Res.* 1999;14(06):2430.
 - [33] Gopalan R, Muraleedharan K, Sastry T, Singh A, Joshi V, Rao DS, Chandrasekaran V. Studies on structural transformation and magnetic properties in Sm₂Co₁₇ type alloys. *J Mater Sci.* 2001;36(17):4117.
 - [34] Fang Y, Chang H, Guo Z, Liu T, Li X, Li W, Chang W, Han B. Magnetic microstructures of phase-separated Sm-Co 2:17-type sintered magnets. *J Alloys Compd.* 2008;462(1):376.
 - [35] Horiuchi Y, Hagiwara M, Okamoto K, Kobayashi T, Endo M, Nakamura T, Sakurada S. Effects of solution treated temperature on the structural and magnetic properties of iron-rich Sm(Co-FeCuZr)_z sintered magnet. *IEEE Trans Magn.* 2013;49(7):3221.
 - [36] Machida H, Fujiwara T, Kamada R, Morimoto Y, Takezawa M. The high squareness Sm-Co magnet having $H_{cb} = 10.6$ kOe at 150 °C. *AIP Adv.* 2017;7(5):056223.
 - [37] Liu J, Hadjipanayis G. Demagnetization curves and coercivity mechanism in Sm(CoFeCuZr)_z magnets. *J Magn Magn Mater.* 1999;195(3):620.
 - [38] Nagamine L, Rechenberg H, Ray A. Fe site populations in Sm₂(Co, Fe)₁₇ and Sm (Co, Fe, Cu, Zr)_{8.35} alloys. *J Magn Magn Mater.* 1990;89(3):270.
 - [39] Feutrill E, McCormick P, Street R. Magnetization behaviour in exchange-coupled-Fe. *J Phys D Appl Phys.* 1996;29(9):2320.
 - [40] Li Z, Zhang M, Shen B, Sun J. Non-uniform magnetization reversal in nanocomposite magnets. *Appl Phys Lett.* 2013;102(10):102405.
 - [41] Yan A, Bollero A, Gutfleisch O, Müller KH. Microstructure and magnetization reversal in nanocomposite SmCo₅/Sm₂Co₁₇ magnets. *J Appl Phys.* 2002;91(4):2192.